SOFT ROBOTICS
Volume 00, Number 00, 2020

DOI: 10.1089/soro.2019.0105

SoRo
Soft Robotics

Design, Modeling, and Evaluation of Fabric-Based Pneumatic Actuators for Soft Wearable Assistive Gloves

Lisen Ge,[1,2] Feifei Chen,[1,2] Dong Wang,[1,2] Yifan Zhang,[1,2] Dong Han,[3–5] Tao Wang,[3–5] and Guoying Gu[1,2]

Abstract

Textile fabrics are compliant, lightweight, and inherently anisotropic, making them promising for the design of soft pneumatic actuators. In this article, we present the design, modeling, and evaluation of a class of soft fabric-based pneumatic actuators (SFPAs) for soft wearable assistive gloves that can simultaneously assist the thumb abduction and finger flexion and extension motions for brachial plexus injury patients. We investigate the mechanical behaviors of various woven fabrics and rib weft-knitted fabric structures, guiding us to design a thumb-abduction SFPA, a finger-flexion SFPA, and a finger-extension SFPA. We further develop a mathematical model to evaluate the influence of the geometric parameters on the blocked tip forces of the finger-flexion SFPAs and extension torques of the finger-extension SFPAs, which are also verified by the experimental results. We then integrate our SFPAs into a soft wearable assistive glove with a portable control system. The glove is finally tested on a healthy volunteer and a brachial plexus injury patient. The clinical evaluation results demonstrate the effectiveness of our designed glove in assisting hand motions and grasping tasks.

Keywords: woven and knitted fabrics, soft fabric-based pneumatic actuators, thumb abduction, finger flexion and extension, soft wearable assistive glove

Introduction

Soft robotics made of soft materials provide exciting opportunities to create a new generation of locomotion[1,2] and manipulation robots,[3] and wearable and assistive soft robots[4] capable of sustaining large deformation while inducing little pressure or damage when interacting with humans or maneuvering through confined spaces. Soft pneumatic actuators are promising in the field of soft robotics owing to their advantages of light weight, low price, and simple actuation.[5,6]

Elastomer materials have been widely used to design different soft pneumatic actuators (such as pneumatic network actuators[7–9] and fiber-reinforced actuators[10,11]) for locomotive robots,[12] robotic grippers[13] and hands,[14] and wearable exoskeleton systems.[15] Recently, many efforts have also been made to design soft wearable gloves for hand rehabilitation and assistance in activities of daily life (ADLs).[16–19] However, the relatively large material weight and low material stiffness of the elastomers lead to small ranges of motions and lower assistive forces, hindering their utility in practical applications. On the other hand, existing soft wearable gloves with elastomer-based actuators generally fail to provide sufficient active extension assistance. Although Heung *et al.*[20] increased the stiffness of the elastomer-based actuators by adding a stainless-steel plate, the required pressure is relatively high and the stainless-steel plate may make the actuators uncomfortable for the wearers.

As an alternative, textile fabric structures that are lighter and stiffer have been recently proposed to design novel soft actuators for wearable gloves.[21–24] For instance, Yap *et al.*[21] exploited woven fabrics and knitted fabrics to design actuators for the assistive glove by providing active extension and flexion assistance, where a folded chamber structure was introduced to enlarge the bending deformation of the flexion actuators. Cappello *et al.*[22] further demonstrated the anisotropy of textile fabrics and investigated soft fabric-based pneumatic actuators (SFPAs) to realize bending and straightening motions by changing the arrangement of the fabric layers. A soft wearable glove was fabricated with the designed SFPAs,[22] and the assistive performance of this glove was clinically

[1]Robotics Institute, School of Mechanical Engineering, Shanghai Jiao Tong University, Shanghai, China.
[2]State Key Laboratory of Mechanical System and Vibration, Shanghai Jiao Tong University, Shanghai, China.
[3]Department of Hand Surgery, Huashan Hospital, Fudan University, Shanghai, China.
[4]Key Laboratory of Hand Reconstruction, Ministry of Health, Shanghai, China.
[5]Shanghai Key Laboratory of Peripheral Nerve and Microsurgery, Shanghai, China.

evaluated on patients suffering spinal cord injury.[23] Connolly *et al.*[24] further established an analytical model to study how the geometric parameters would affect the deformation of the SFPAs for a wearable glove.

Despite the impressive achievements, researches on SFPAs have just been at an initial step and have several limitations. First, current SFPAs mainly focus on flexion and extension assistance for the fingers, while little attention is paid to the thumb abduction assistance. In fact, the dexterous thumb motions play an essential role in most grasping tasks in ADLs.[25] As shown in Figure 1a and b, the thumb abduction motion is important because it determines the grasping width (Fig. 1c).[26] Unfortunately, it is prone to damage after many diseases and injuries, such as brachial plexus injury, resulting in adduction distortion of the thumb (Fig. 1c). Second, the varied requirements of assistive forces for the impaired hands caused by different diseases and injuries raise the need for a thorough understanding of the output forces of SFPAs. However, few works have quantitatively studied the effects of the geometric parameters on the assistive forces of SFPAs.

In this article, we present the design, modeling, and evaluation of a class of SFPAs for soft wearable gloves to simultaneously assist the thumb abduction and finger flexion and extension motions.

The mechanical behaviors of various woven fabrics and rib weft-knitted fabrics are experimentally investigated first to select materials for the SFPAs. We next design the flexion and extension SFPAs to assist the fingers for closing and opening movements and further develop an independent SFPA to abduct the thumb to the functional position of the hand. We also develop a mathematical model to investigate the effects of geometric parameters on the blocked tip forces of the finger-flexion SFPAs and the extension torques of the finger-extension SFPAs, which are further verified by the experimental results.

Finally, by integrating the thumb-abduction SFPA and finger-flexion and finger-extension SFPAs, a soft wearable assistive glove is integrated. Experiments are conducted to evaluate the ranges of the assistive motions and forces of the glove. The results demonstrate that a brachial plexus injury patient with thumb adduction distortion with our soft wearable assistive glove successfully restores the hand functions in opening the hand and accomplishing several grasping tasks in ADLs.

The remainder of this work is organized as follows. The next section first presents the material characterization and selection for the SFPAs, and then demonstrates the design and modeling of the thumb-abduction SFPA and finger-flexion and finger-extension SFPAs. In the Integration and Evaluation section, the SFPAs are integrated into a soft wearable glove, and the glove is characterized by its assistive capabilities. This section further shows the clinical evaluation results of the glove. Finally, the Conclusion section concludes this work.

Design and Modeling

Material characterization and selection for the SFPAs

In this work, we select textile fabrics coated with thermoplastic polyurethane (TPU) film for design of the SFPAs. As shown in Figure 2a, this material has a two-layer structure, in which the textile fabric layer provides anisotropic mechanical properties,[22] while the TPU film layer is coated on one side of the textile fabric to prevent air leakage. The overall thickness of the material is less than 0.5 mm, making the material light, complaint, and compatible with human body motions.

Textile fabrics are commonly produced by weaving and knitting methods.[27] Woven fabrics consist of orthogonal interlacing warp threads and weft threads (Fig. 2b—1).[27] The warp threads run along the length direction of the fabric, while the weft threads are along the width direction. Knitted fabrics are produced by interlocking loops of the threads and can be classified into the warp-knitted type (Fig. 2b—2) and weft-knitted type (Fig. 2b—3),[28] depending on the loop directions.

Woven fabrics typically have a higher elastic modulus and lower mechanical compliance than their knitted counterparts because of the tightly interlaced structures, as shown in Figure 2c and d.[27] The linear density of the warp threads in woven fabrics is typically higher than the weft threads, leading to their anisotropic mechanical properties.

On the contrary, knitted fabrics present larger extensibility and more significant anisotropy than woven fabrics because of their looped structuring (Fig. 2e).[28] Specifically, weft-knitted fabrics are usually more extensible than warp-knitted

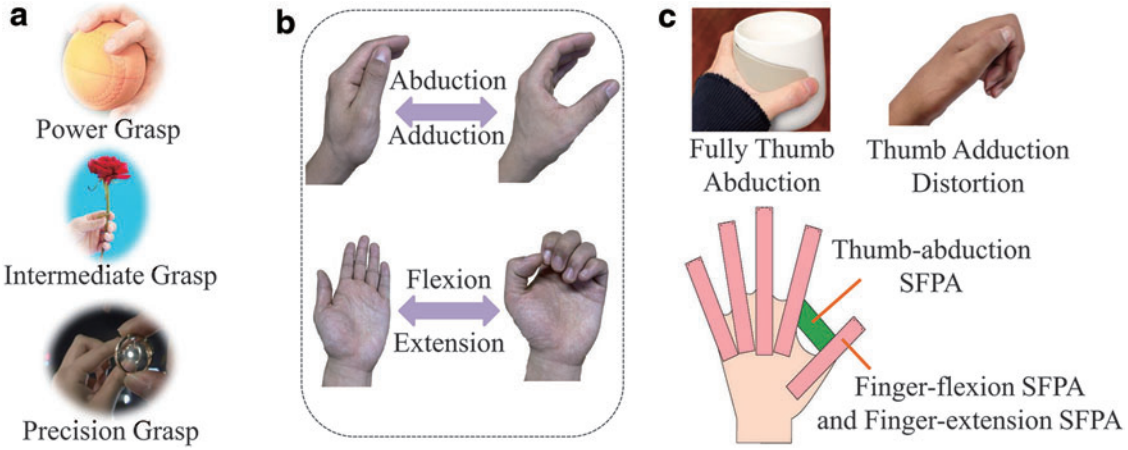

FIG. 1. Schematics of basic hand motions in ADLs and the corresponding requirements for hand rehabilitation and assistive functions. **(a)** The three main grasps and gestures of the hand in ADLs. **(b)** The main finger motions in the three grasps. **(c)** The required actuators of a soft wearable glove for hand function assistance in ADLs. ADL, activity of daily life; SFPA, soft fabric-based pneumatic actuator. Color images are available online.

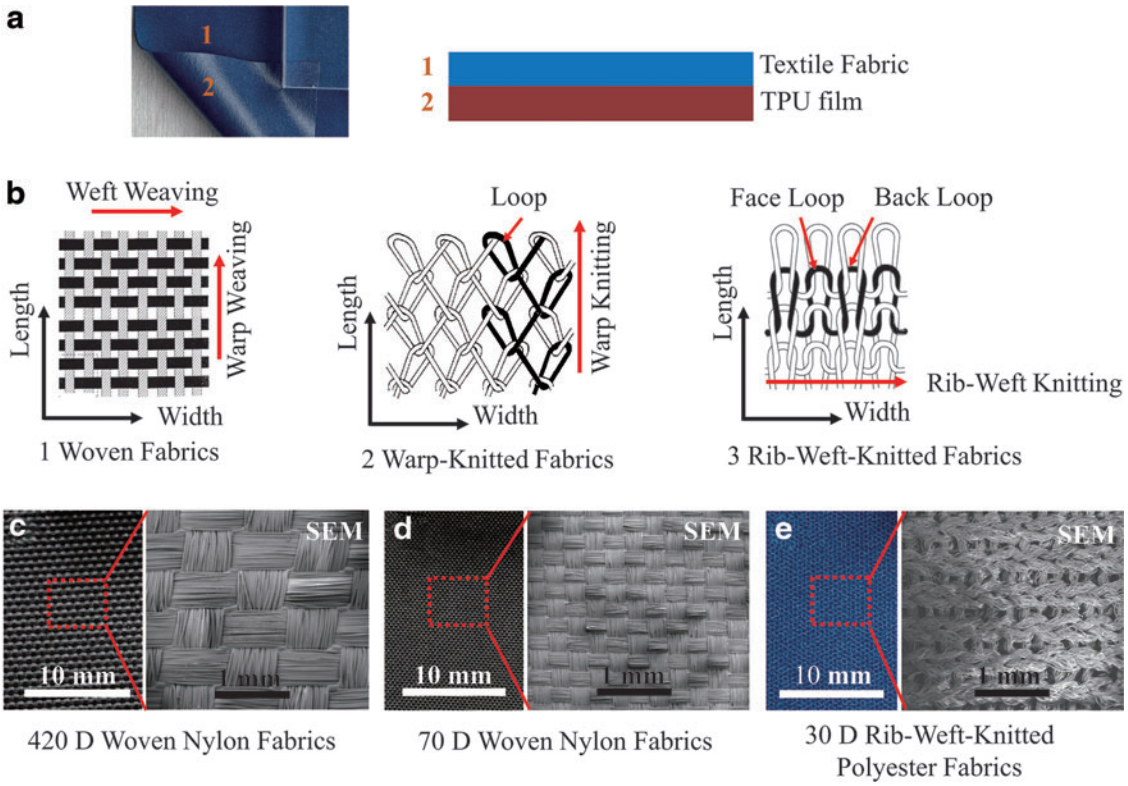

FIG. 2. Schematics of the materials for the fabrication of the SFPAs. **(a)** The structure of the material. **(b)** Constructions of woven fabrics,[27] warp-knitted fabrics,[28] and rib weft-knitted fabrics.[29] **(c–e)** Digital photos and SEM pictures of the 420 denier (D) woven nylon fabric, 70 D woven nylon fabric, and 30 D rib weft-knitted polyester fabric. SEM, scanning electronic microscope; TPU, thermoplastic polyurethane. Color images are available online.

fabrics. However, weft-knitted fabrics with asymmetric structures such as plain weft-knitted fabrics tend to curl and may cause difficulties in fabricating SFPAs. Therefore, the rib weft-knitted fabrics are more suitable since their face loops and back loops (Fig. 2b—3) alternate to form a more stable structure that is less prone to curl. Furthermore, the textile fabrics can be produced using fibers of different thicknesses (in denier, D).[30] The fabrics with a higher denier are thicker (Figs. 2c, d) and sturdier.

To quantitatively compare the mechanical behaviors of the woven fabrics and rib weft-knitted fabrics, we conduct uniaxial tensile tests on the 420 D woven nylon fabric (coated with 0.1 mm TPU film; Jiaxing Inch Eco-Materials) and 30 D rib weft-knitted polyester fabric (coated with 0.2 mm TPU film), according to the ASTM D5034-09 standard. We make rectangular specimens (100 × 50 mm), and set the tensile speed to be 300 mm · min^{-1}.

We can see from Figure 3a that the elongations-until-failure for the 420 D woven nylon fabric are 53.3% at 1701.2 N in the warp direction and 62.8% at 1155.2 N in the weft direction. The results in Figure 3b show that the elongations-until-failure of the 30 D rib weft-knitted polyester fabric in the warp direction and weft direction are 99.2% at 328.3 N and 375.7% at 268.3 N, respectively. It is found that the 30 D rib weft-knitted polyester fabric can achieve larger extension than the 420 D woven nylon fabric in both warp and weft directions. Besides, both types of fabrics are stiffer in their warp directions.

To investigate the effect of the fiber thickness on the mechanical behaviors of the textile fabrics, we conduct uniaxial

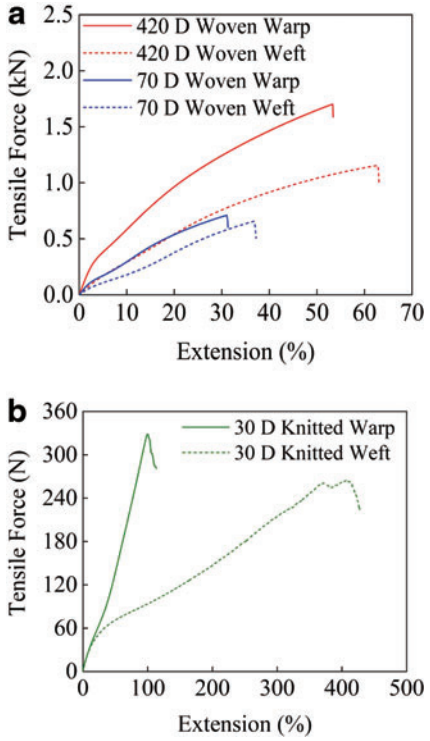

FIG. 3. Characterizations of the materials for the fabrication of the SFPAs. **(a)** Tensile test results of the 420 and 70 D woven nylon fabrics. **(b)** Tensile test results of the 30 D rib weft-knitted polyester fabric. Color images are available online.

tensile tests on the 70 D woven nylon fabric (coated with 0.1 mm TPU film) and compare the test results with the 420 D woven nylon fabric. As shown in Figure 3a, the 70 D woven nylon fabric can achieve a maximum extension of 31.0% at 709.9 N in the warp direction and 36.8% at 657.5 N in the weft direction. It is observed that woven fabrics with a higher denier are stiffer and able to withstand larger extension in both warp and weft directions.

Based on the tensile test results, we select the stiffer and less extensible 420 D woven nylon fabric for the thumb-abduction SFPA to provide sufficient abduction force and preserve the abduction angle around the functional position of hands. The finger-extension SFPAs assist the extension of the initially clenched fingers, and require higher stiffness to provide sufficient extension torques. To this end, we choose the 420 D woven nylon fabric for the finger-extension SFPAs. On the contrary, we utilize the softer and more extensible 30 D rib weft-knitted polyester fabric for the finger-flexion SFPAs to generate sufficient bending deformation under low pressurization.

Thumb-abduction SFPA

In human anatomy, the thumb abduction is defined as the movement of the thumb anteriorly perpendicular to the palm,[31] and is measured by the angle between the axis of the first metacarpal and the second metacarpal (Fig. 4a), denoted by θ.[32] The thumb abduction angle can be adjusted for different grasping tasks. We take the functional position of the hand (Fig. 4a) as the reference state since most functions of the hand are performed here,[33,34] with the thumb abduction angle θ ranging from 40° to 60°,[32] and the metacarpophalangeal (MCP) joint flexion angle ϕ ranging from 30° to 45°.[33]

Considering the thumb abduction and adduction postures in Figure 1c, we arrange the thumb-abduction SFPA between the thumb and the index finger. The selected fabric is sufficiently compliant to allow the thumb-abduction SFPA to reconfigure freely and adjust to the adduction motion of the thumb at a low level of pressurization. As the input pressure increases, the thumb-abduction SFPA becomes stiffer and tends to straighten, thus generating a force to abduct the thumb.

As shown in Figure 4a, we design a quadrilateral thumb-abduction SFPA. The proximal end is set to be in line with the first MCP joint and the second MCP joint. To avoid inducing additional constraints to the hand motion, the dimensions of the thumb-abduction SFPA conform to the thumb and the index finger. Therefore, the distal end is aligned with the first interphalangeal (IP) joint and the second proximal interphalangeal (PIP) joint. After some experimental tests, we set $\theta = 50°$ and $\phi = 37.5°$ to determine the final shape of the thumb-abduction SFPA.

The thumb-abduction SFPA consists of a top woven fabric layer, a bottom woven fabric layer, and a spacer in between. To enhance the stiffness of the actuator, the warp direction of the fabric is set aligned with the thumb abduction direction. The spacer made of neoprene sponge (1.5 mm thick; Dongguan VF Industrial) allows fluent airflow.

The main processes of fabricating the thumb-abduction SFPA are illustrated in Figure 4b. First, the two fabric layers and one spacer are shaped by laser cutting (VLS 3.50; Universal Laser Systems). Then, the spacer is sandwiched between the two fabric layers that are thermally welded along their four edges later with an impulse sealer (PFS-650*2; Dongguan Xiang Bo Electromechanical Equipment). Finally, one polyurethane tube is connected and glued for air outlets. In the thermal welding process, the spacer isolates the top and bottom fabric layers to form the geometric shape of the chamber, which also guarantees the consistency of the actuators. As illustrated in Figure 4c, two fabric layers and one spacer form one thumb-abduction SFPA with an overall width W_o and a chamber width W, with their difference being the width of the sealing edge, that is, 5 mm in this work.

To evaluate the design of the thumb-abduction SFPA, we develop a finite element model with ABAQUS (6.14-4; Dassault Systèmes S.A) to study its deformation under pressurization. The actuator is simplified to be rectangular and initially folded in the finite element model, with geometric parameters shown in Figure 5a. The modeling process mainly includes three steps:

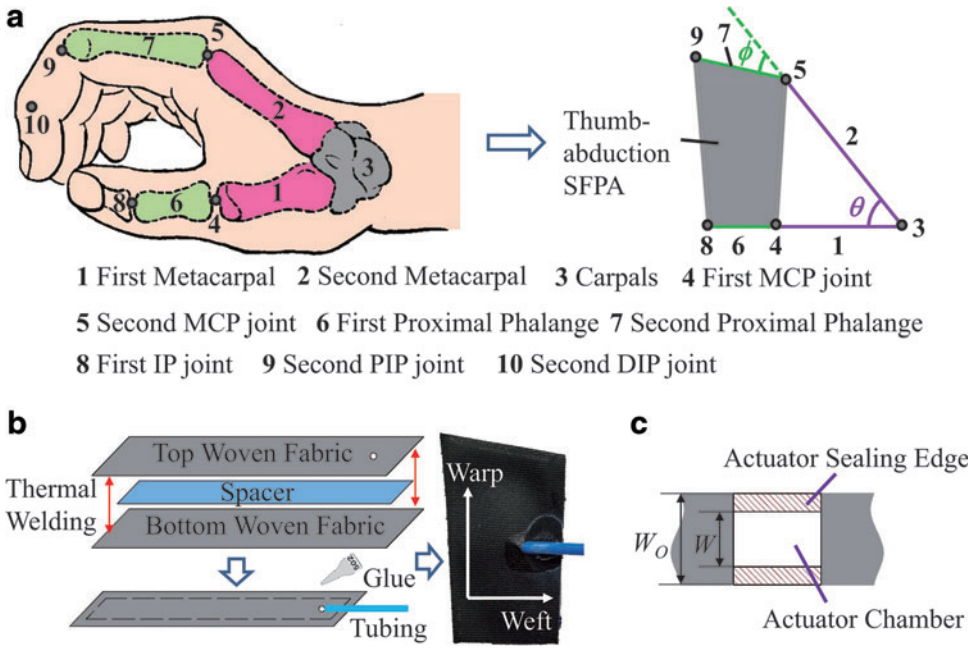

FIG. 4. Design and fabrication of the thumb-abduction SFPA. **(a)** Functional position of the hand [33] and the design of the thumb-abduction SFPA. **(b)** The main fabrication process of the thumb-abduction SFPA and the fabricated actuator in the deflated state. **(c)** The overall width W_o and chamber width W of the thumb-abduction SFPA. DIP, distal interphalangeal; IP, interphalangeal; MCP: metacarpophalangeal; PIP, proximal interphalangeal. Color images are available online.

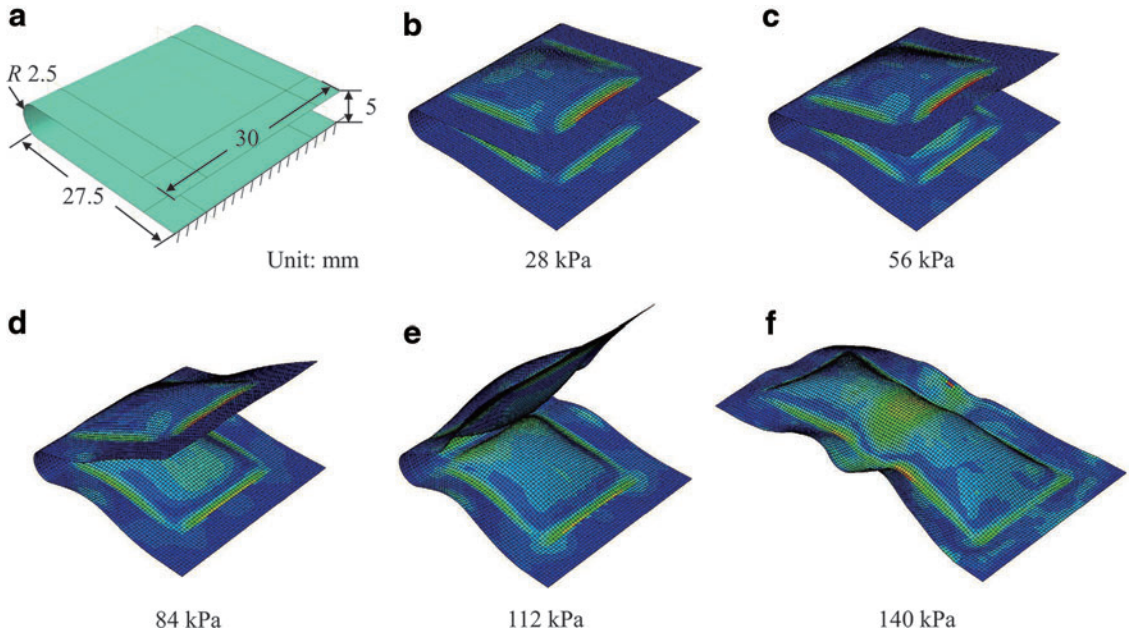

FIG. 5. Finite element simulation of the thumb-abduction SFPA. **(a)** The geometric model of the initially folded thumb-abduction SFPA. **(b–f)** Simulation results of the unfolding motion of the thumb-abduction SFPA under different levels of pressurization. Color images are available online.

(1) The geometric model is meshed by the 4-node reduced shell elements.
(2) For the material properties, the 420 D woven nylon fabric is modeled by an anisotropic material and is captured by the lamina model in ABAQUS. The parameters of the lamina model are determined according to Glaser's work,[35] that is, the Young's moduli $E_1 = 394$ MPa, $E_2 = 145.5$ MPa, the Poisson's ratio $\mu_{12} = 0.23$, and the shear moduli $G_{12} = 14.6$ MPa, $G_{13} = 14.6$ MPa, $G_{23} = 14.6$ MPa, with the subscripts 1, 2, 3 denoting the warp, weft, and surface normal directions of the fabric. The density of the fabric is 1.14×10^{-3} g · mm^{-3}.
(3) The input pressure is set to be 140 kPa. As shown in Figure 5a, the thumb-abduction SFPA is constrained at the bottom edge.

The simulation is conducted using the dynamic explicit solver in ABAQUS. It is observed that the thumb-abduction SFPA gradually unfolds with the increasing input pressure until it fully straightens, as shown in Figure 5b–f.

The performance of the thumb-abduction SFPA is characterized by its assistive abduction force and range of abduction motion. As shown in Figure 6a, we set up a measurement platform to evaluate the abduction force. The thumb-abduction

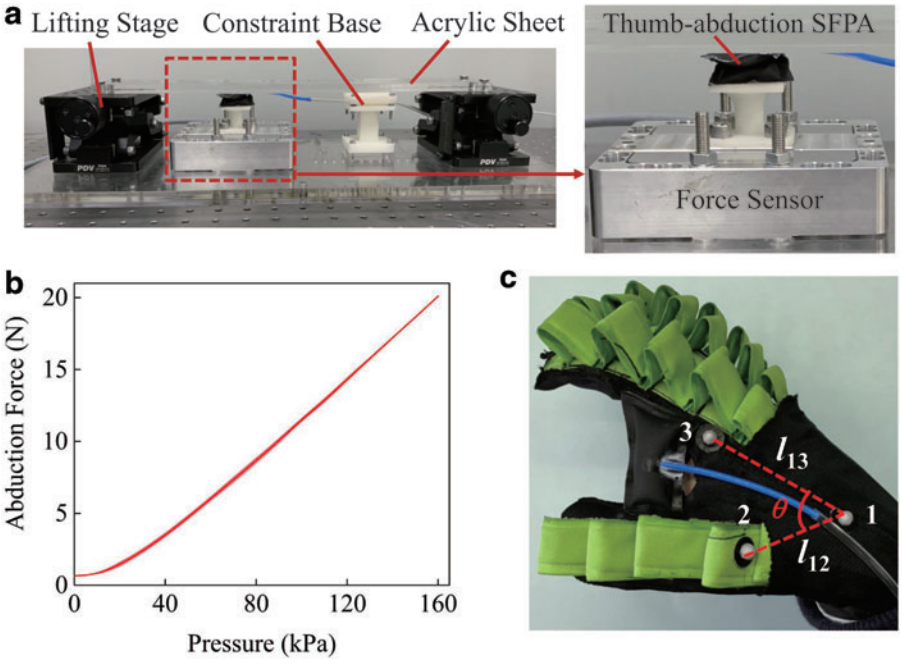

FIG. 6. Characterization of the thumb-abduction SFPA. **(a)** Experimental setup for the abduction force of the thumb-abduction SFPA. **(b)** Experimental results of the abduction force of the actuator with the increase of the input pressure for three times, together with the error bands in light color regions. **(c)** Evaluation of the assistive abduction angle of the thumb-abduction SFPA on a soft wearable glove. Color images are available online.

SFPA is supported by the force sensor (K3D120; ME-Messsysteme) and constrained at its connection tube. During pressurization, the top acrylic sheet (10 mm thick) blocks the straightening motion of the actuator, and thus, the actuator outputs an abduction force to the sensor. The lifting stages (PT-SD408S; PDV) support the sheet and adjust the height of the sheet. In the tests (three times), the input pressure increases from 0 to 160 kPa with a step of 10 kPa. The experimental results in Figure 6b show that the abduction force increases almost linearly with the input pressure, reaching up to 20.1 N under 160 kPa input pressure.

We further evaluate the abduction motion range of the actuator on a soft wearable glove. As shown in Figure 6c, the thumb-abduction SFPA abducts the thumb to the functional position when the input pressure is 50 kPa. We set three markers at the carpals (Marker 1), the first MCP joint (Marker 2), and the second MCP joint (Marker 3), and measure the thumb abduction angle θ, that is, the angle between l_{12} and l_{13}, by three times. The data are processed using the software ImageJ (National Institutes of Health), with the calculated abduction angle reaching up to 50.5°.

Finger-flexion SFPAs

To generate bending deformation to assist finger flexion, we design a two-layer finger-flexion SFPA by arranging the fabrics of the top and bottom layers orthogonally (knitted weft and knitted warp), with the whole length being 140 mm and the chamber width 15 mm, as shown in Figure 7a. It is found that the two-layer finger-flexion SFPA can achieve considerable bending deformation, but requires quite high input pressure, that is, up to 200 kPa, which may cause safety issues when interacting with humans and limit the portability of the power source.

To minimize the required input pressure, we design the structure of the finger-flexion SFPA by folding its chamber to form a bellow structure and subsequently welding the folded chamber onto a third limiting layer. We further develop an approach to determine the length of the folded chamber. The bellows may be irregular in shape because of the high compliance of the fabrics. To describe the bellow shape and determine the chamber length L_t, we assume the bellow shape is an isosceles triangle. As shown in Figure 7b, the bellow height h, span a, spacing b, and distal end length L_d of the folded chamber are set to be 10, 10, 5, and 15 mm, respectively. The proximal end length L_p is constrained to be not less than 15 mm to ensure fabrication quality. The actuator length L is set to be 140 mm to fit the finger length of human hands. The chamber width W is set to be 15 mm. The bellow number n of the folded chamber is determined according to the constraints

$$\begin{cases} L = L_d + n \cdot a + (n-1) \cdot b + L_p \\ L_p \geq 15 \text{ mm} \end{cases}. \tag{1}$$

By solving Eq. (1), we obtain $n = 7$. As shown in Figure 7b, the chamber length L_t is

$$L_t = L + \left(\sqrt{5} - 1\right) \cdot a \cdot n = 226.5 \text{ mm}. \tag{2}$$

When fabricating the finger-flexion SFPA, the top chamber is first manufactured with the same approach as that of the thumb-abduction SFPA. As shown in Figure 7b, the knitted weft direction of the fabric is aligned with the length direction

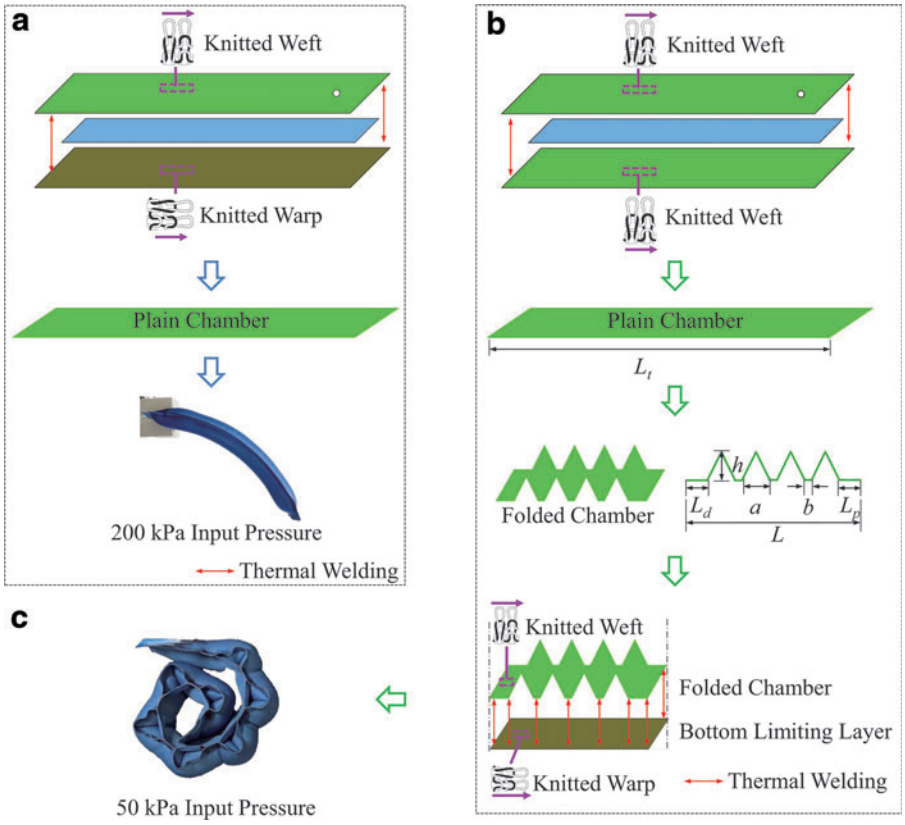

FIG. 7. Design and fabrication of the finger-flexion SFPA. **(a)** The fabrication process of a two-layer finger-flexion SFPA and the bending deformation of the actuator under 200 kPa input pressure. **(b)** The geometric parameters of the folded chamber and the main fabrication process of the finger-flexion SFPA with the top folded chamber. **(c)** The bending deformation of the finger-flexion SFPA with the folded chamber under 50 kPa input pressure. Color images are available online.

of the top chamber. The top chamber is subsequently folded to the designed shape based on the aforementioned geometric parameters. The folded chamber is welded onto the bottom limiting layer using a heat presser. In this process, the proximal end, distal end, and the gaps between two adjacent bellows of the folded chamber are welded onto the bottom limiting layer. The knitted warp direction is aligned with the length direction of the bottom limiting layer. The results in Figure 7c show that the fabricated finger-flexion SFPA can achieve a bending angle of nearly 360° under 50 kPa input pressure.

The blocked tip force that determines the assistive grasping force of the soft wearable glove is another important performance indicator of the finger-flexion SFPA. We develop a mathematical model to understand how the geometric parameters influence the blocked tip force of the finger-flexion SFPA.

In the blocked tip force test, the finger-flexion SFPA is constrained at its proximal end and supported by the force sensor at its distal end, as shown in Figure 8a. While inflating, the input pressure exerts a force $\mathbf{F_i}$ on the distal end of the finger-flexion SFPA. Because of the limiting layer and the geometric asymmetry of the folded chamber, the action line of the $\mathbf{F_i}$ has an eccentric distance e from the neutral axis. Therefore, the axial force $\mathbf{F_i}$ generates a bending moment M_{Fi} on the finger-flexion SFPA and hence outputs a blocked tip force $\mathbf{F}$ on the force sensor. The force sensor provides a counterforce to balance the bending moment M_{F}. We can obtain

$$\begin{cases} M_{\mathrm{Fi}} = |\mathbf{F_i}| \cdot e \\ M_{\mathrm{F}} = |\mathbf{F}| \cdot L \\ M_{\mathrm{Fi}} = M_{\mathrm{F}} \end{cases}, \tag{3}$$

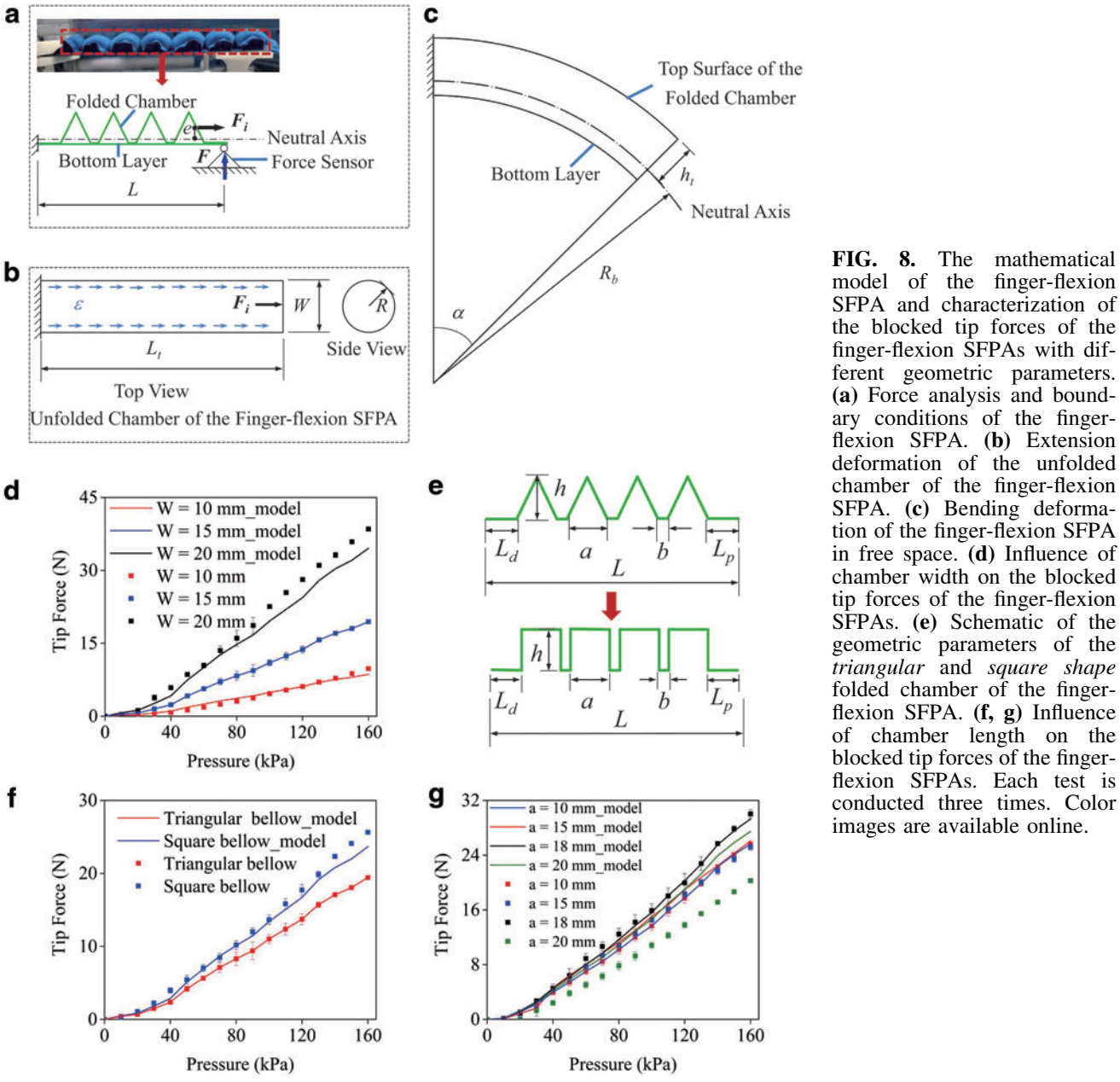

FIG. 8. The mathematical model of the finger-flexion SFPA and characterization of the blocked tip forces of the finger-flexion SFPAs with different geometric parameters. **(a)** Force analysis and boundary conditions of the finger-flexion SFPA. **(b)** Extension deformation of the unfolded chamber of the finger-flexion SFPA. **(c)** Bending deformation of the finger-flexion SFPA in free space. **(d)** Influence of chamber width on the blocked tip forces of the finger-flexion SFPAs. **(e)** Schematic of the geometric parameters of the *triangular* and *square shape* folded chamber of the finger-flexion SFPA. **(f, g)** Influence of chamber length on the blocked tip forces of the finger-flexion SFPAs. Each test is conducted three times. Color images are available online.

and thus

$$|\mathbf{F}| = \frac{|\mathbf{F_i}| \cdot e}{L}. \tag{4}$$

The top chamber of the finger-flexion SFPA generates extension under the axial force $\mathbf{F_i}$, as shown in Figure 8b. Since the knitted weft direction is along the length direction of the top chamber, the chamber is much stiffer in the transverse direction. We therefore assume the extension only occurs at the length direction of the chamber. The axial force is

$$|\mathbf{F_i}| = P \cdot A, \tag{5}$$

where P is the input pressure, and A is the cross-sectional area of the inflated chamber. We assume that the cross section of the chamber is a circle with a radius R for ease of analysis, as in Cappello *et al.*'s work[22] and Connolly *et al.*'s work.[24] Therefore, the axial force is

$$|\mathbf{F_i}| = P \cdot \pi \cdot R^2. \tag{6}$$

Since the finger-flexion SFPA generates no transverse extension, the relationship between the chamber width W and the radius R is

$$R = \frac{W}{\pi}. \tag{7}$$

Substituting Eq. (7) into Eqs. (6) and (4), we obtain

$$|\mathbf{F}| = P \cdot W^2 \cdot e/(\pi \cdot L). \tag{8}$$

On the other hand, the length of the folded chamber determines its overall extension, and thus influences the blocked tip force. The extension of the folded chamber is

$$\Delta L_t = L_t \cdot \varepsilon, \tag{9}$$

where ε is the extension strain of the chamber. Considering the bending deformation of the finger-flexion SFPA in free space, as shown in Figure 8c, the extension of the folded chamber leads the finger-flexion SFPA to bend toward the bottom limiting layer with a radius R_b and a bending angle α. According to the Euler–Bernoulli beam theory,[36]

$$\Delta L_t = (R_b + h_t) \cdot \alpha - R_b \cdot \alpha, \tag{10}$$

where h_t is the distance between the top surface of the folded chamber and the neutral axis (Fig. 8c). Substituting Eq. (10) into (9), we obtain

$$\alpha = \frac{L_t \cdot \varepsilon}{h_t}. \tag{11}$$

To constrain the bending deformation, the reaction moment M_F that the force sensor provides is

$$M_F = \frac{K \cdot \alpha}{L} = K \cdot \frac{L_t \cdot \varepsilon}{h_t \cdot L}, \tag{12}$$

where K is the bending stiffness of the finger-flexion SFPA. Substituting Eq. (12) into (3), we have

$$|\mathbf{F}| = K \cdot \frac{L_t \cdot \varepsilon}{h_t \cdot L^2}. \tag{13}$$

The extension strain ε mainly depends on the elastic modulus E of the folded chamber and the input pressure. Therefore, according to Eqs. (8) and (13), with the parameters L, e, h_t fixed, the blocked tip force is proportional to L_t and the square of W, which later will be verified by experiments.

For ease of analysis, we set the finger-flexion SFPA with geometric parameters above (Table 1) as the reference finger-flexion SFPA (flexion-SFPA-0). Then we fabricate finger-flexion SFPAs with $W = 10$ mm (flexion-SFPA-1) and $W = 20$ mm (flexion-SFPA-2) while keeping the other parameters unchanged (Table 1), and test the blocked tip forces of the three actuators with the input pressure increasing from 0 to 160 kPa with a step of 10 kPa. We estimate the blocked tip forces of flexion-SFPA-1 and flexion-SFPA-2 based on the experimental result of the flexion-SFPA-0, which is

$$|\mathbf{F}_v| = |\mathbf{F}_r| \cdot \left(\frac{W_v}{W_r}\right)^2, \tag{14}$$

where subscripts v and r represent the estimated and reference quantities, respectively, and similarly hereinafter. The magnitudes of $\mathbf{F}_r$ under different input pressures are obtained from the average of the experimental results directly.

The results in Figure 8d demonstrate that flexion-SFPA-0, flexion-SFPA-1, and flexion-SFPA-2 can provide blocked tip forces of 19.4, 9.8, and 38.5 N, respectively, under an input pressure of 160 kPa. The corresponding model-predicted results for flexion-SFPAs-1 and 2 are 8.6 and 34.6 N, which agree well with the experimental results.

Table 1. Geometric Parameters of the Tested Finger-Flexion Soft Fabric-Based Pneumatic Actuators

	Bellow shape	L *(mm)*	W *(mm)*	L_d *(mm)*	h *(mm)*	a *(mm)*	b *(mm)*	L_p *(mm)*	n	L_t *(mm)*
Flexion-SFPA-0	Triangular	140	15	15	10	10	5	20	7	226.5
Flexion-SFPA-1	Triangular	140	10	15	10	10	5	20	7	226.5
Flexion-SFPA-2	Triangular	140	20	15	10	10	5	20	7	226.5
Flexion-SFPA-3	Square	140	15	15	10	10	5	20	7	280
Flexion-SFPA-4	Square	140	15	15	18	18	5	15	5	320
Flexion-SFPA-5	Square	140	15	15	15	15	5	30	5	290
Flexion-SFPA-6	Square	140	15	15	20	20	5	30	4	300

SFPA, soft fabric-based pneumatic actuator.

We subsequently investigate the influence of the chamber length L_t on the blocked tip force of the finger-flexion SFPA. For a finger-flexion SFPA with fixed actuator length L, the chamber length L_t mainly depends on the bellow shape. As mentioned above, the chamber length of flexion-SFPA-0 is determined based on an isosceles triangle. However, the isosceles triangle may not make full use of the bellow span. Inspired by the rectangular chamber structure of the pneumatic network actuators,[5] we redesign the bellow of a rectangular shape, as shown in Figure 8e. Similarly, we set $h = a$ to preserve the height and span ratio of the bellow. The rectangle bellow is therefore a square one. The chamber length is

$$L_t = L + 2 \cdot a \cdot n. \tag{15}$$

With all the other geometric parameters the same with flexion-SFPA-0, we design another finger-flexion SFPA (flexion-SFPA-3) with square bellows (Table 1), and predict its blocked tip force by

$$|\mathbf{F}_v| = |\mathbf{F}_r| \cdot \frac{L_{t,v}}{L_{t,r}}. \tag{16}$$

The experimental results are largely in line with the model-predicted results (Fig. 8f) and show that flexion-SFPA-3 can provide a blocked tip force of 25.6 N, under 160 kPa input pressure.

Furthermore, we study how to select the bellow height h and span a to maximize the chamber length L_t with the given actuator length L. Considering the requirement of the soft robotic glove,[17] we set the maximum value of the bellow height to be 20 mm. The constraints are summarized as follows:

$$\begin{cases} L = 140 \text{ mm} \\ b = 5 \text{ mm} \\ L_{\mathrm{d}} = 15 \text{ mm} \\ L_{\mathrm{p}} \geq 15 \text{ mm} \\ h \leq 20 \text{ mm} \\ h = a \end{cases}. \tag{17}$$

As shown in Figure 8e, the chamber length is

$$L_t = L_d + n \cdot 3a + (n-1) \cdot b + L_p. \tag{18}$$

By solving Eqs. (15), (17), and (18), we obtain $a = 18$ mm, $n = 5$, and $L_t = 320$ mm. We further fabricate three finger-flexion SFPAs with parameters $a = 18$ mm (flexion-SFPA-4), $a = 15$ mm (flexion-SFPA-5), and $a = 20$ mm (flexion-SFPA-6) (Table 1). By setting flexion-SFPA-3 as the reference, we use the established model to predict their blocked tip forces and conduct experiments for validation. The experimental results in Figure 8g show that the flexion-SFPA-4 can achieve the largest blocked tip force, that is, 30.03 N under an input pressure of 160 kPa. The model-predicted result is 29.3 N, which agrees well with the experimental finding.

Although the model predicts that flexion-SFPA-6 can generate larger blocked tip force than flexion-SFPA-3 and flexion-SFPA-5, the experimental results are opposite. This discrepancy can be caused by the influence of other parameters, such as the bellow number n. As shown in Table 1, flexion-SFPA-3 and flexion-SFPA-5 contain five bellows, while flexion-SFPA-6 only has four bellows. The current model can be further improved by considering more factors.

Finger-extension SFPAs

The working principle of a finger-extension SFPA uses the stiffness change of its body. When deflated, the finger-extension SFPA is flexible enough to conform to the curved finger. After inflation, the finger-extension SFPA becomes stiffer and tends to straighten, thus generating an extension force and an extension torque. We fabricate the finger-extension SFPA using the same approach as that of the thumb-abduction SFPA. As shown in Figure 9a, while fabricating the finger-extension SFPA, we align the warp direction of the fabric with the length direction of the actuator.

The extension torque $\mathbf{T}$ is the main parameter to characterize the performance of the finger-extension SFPA, determined by

$$\mathbf{T} = \mathbf{r} \times \mathbf{F_e}, \tag{19}$$

where $\mathbf{F_e}$ and $\mathbf{r}$ are the vectors of the extension force and the force arm. We first set the initial flexion angle to be 60° and study the influence of geometric parameters on the extension torque. Similarly, we develop a simple mathematical model to predict the extension torque, which is

$$|\mathbf{T}_v| = |\mathbf{T}_r| \cdot \left(\frac{W_v}{W_r}\right)^2. \tag{20}$$

We set up a test rig to measure the extension torques, as shown in Figure 9b. The test rig includes a torque sensor (TFF400; FUTEK) and a precision rotation guide (RSP 125-L; Dongguan Shengling precision machinery). The rotation guide can provide varied initial flexion angles for the finger-extension SFPAs.

We measure the extension torques of three finger-extension SFPAs with the chamber width $W = 15$ mm (reference extension SFPA), $W = 10$ mm (extension-SFPA-1), and $W = 20$ mm (extension-SFPA-2). In the tests, the input pressure increases from 0 to 160 kPa with a step of 10 kPa. The experimental results in Figure 9c show that the reference extension SFPA, extension-SFPA-1, and extension-SFPA-2 can provide 0.94, 0.43, and 1.51 N · m extension torques when the input pressure is 160 kPa, respectively. The corresponding model-predicted results for the extension-SFPA-1 and extension-SFPA-2 are 0.42 and 1.67 N · m. The model-predicted results agree well with the experimental results for extension-SFPA-1 and with acceptable discrepancy for extension-SFPA-2.

We finally study the influence of the initial flexion angle on the extension torque using the reference extension SFPA. The input pressure is set to be 160 kPa. The initial flexion angle increases from 15° to 120° with a step of 15°. The results in Figure 9d interestingly show that, with the increase of the initial flexion angle, the extension torque first increases, peaks at 45°, and then decreases due to the stiffening of the inflated finger-extension SFPA. After inflation, the initially compliant finger-extension SFPA becomes stiffer and cannot undergo too large flexion angle. Once the flexion angle becomes overlarge, creases may occur on the finger-extension SFPA, and the chamber is folded into two discrete segments. Nevertheless,

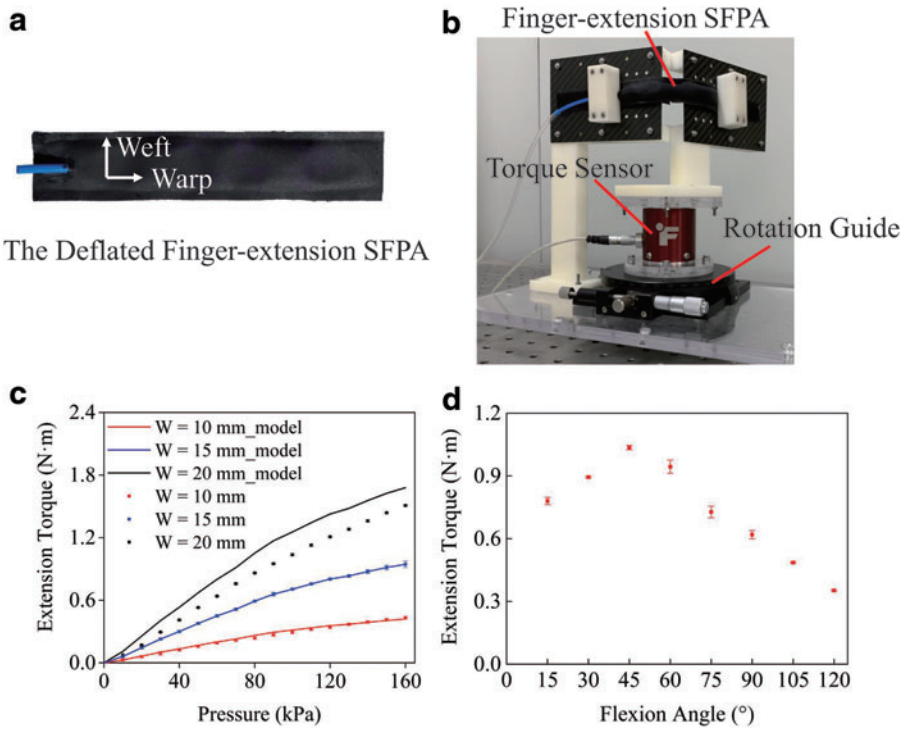

FIG. 9. Design and characterization of the finger-extension SFPAs. **(a)** Fabric orientation arrangement of the finger-extension SFPA. **(b)** Test rig for the extension torque of the finger-extension SFPA. **(c, d)** Influence of the chamber width, and initial flexion angle on the extension torque of the finger-extension SFPAs. The input pressure for the results in **(d)** is 160 kPa. Each test is conducted three times. Color images are available online.

the finger-extension SFPA can provide an extension torque of 0.35 N · m when the initial flexion angle is 120°.

Integration and Evaluation

Integrating SFPAs into soft wearable assistive gloves

The soft wearable assistive glove is designed open-palm for ease of donning and doffing. The glove base part is made of Spandex coated with 1.5-mm-thick neoprene sponge (Dongguan VF Industrial). This deformable material enables the glove to extend to minimize its mechanical impedance to the motion of fingers. Based on the characterization results of the SFPAs, we integrate the designed thumb-abduction SFPA and finger-flexion and finger-extension SFPAs into the glove. We set the chamber width of the finger-flexion and finger-extension SFPAs to be 15 mm. The lengths of the actuators are customized for one healthy volunteer.

The integration process mainly contains four steps (Fig. 10a). First, the bottom limiting layers of the five finger-flexion SFPAs are sewn on the dorsal side of the glove base. Second, the top folded chambers of the finger-flexion SFPAs are thermally welded onto the bottom limiting layers. Subsequently, the finger-extension SFPAs are arranged at the palm side of the glove base. The whole body of each finger-extension SFPA is anchored to the glove base via hoops and loops. The proximal and distal ends of the finger-flexion and finger-extension SFPAs are sewn on the glove base to ensure fitness and firmness. The finger-extension SFPA on each finger is set to be 10 mm longer than the finger-flexion SFPA to avoid puncturing the finger-flexion SFPA during sewing. Finally, the two side edges of the thumb-abduction SFPA are sewn onto the dorsal side of the glove base. The fabricated soft wearable assistive glove is demonstrated in Figure 10b with an overall weight of 128 g, which is much lighter than the upper limit weight (around 500 g).[17]

The control system of the glove is packaged into a portable instrument box to reduce the weight on the upper limb (Fig. 10c). The control system mainly consists of the electronics, the pneumatic components, and the power components. The electronics include a microcontroller (Arduino Uno, Arduino), a 1-bit relay (CF008; Omron), an 8-bit relay (CF008; Omron), and a Bluetooth module (HC-05; Qi Xing Chong). The pneumatic components contain two miniature pneumatic pumps (CTS series; Parker), seven miniature solenoid valves (X-Valve; Parker), and three air pressure sensors (XGZP6847; HAD Electronic). The power components include two 3.7 V lithium batteries (18650; Panasonic) in series for the electronics and one 12 V lithium battery (20C; GREPOW) for the pneumatic components.

The microcontroller controls the activation and deactivation of the pumps and valves through the relays. The activation and deactivation switches of the pumps and the valves modulate the inflation and deflation of the actuators. In this sense, we can independently control the thumb-abduction SFPA and each finger-flexion SFPA. The five finger-extension SFPAs are controlled to be on and off simultaneously. Three air pressure sensors monitor the input pressure that is supplied to the thumb-abduction SFPA and finger-flexion and finger-extension SFPAs, respectively. The microcontroller regulates the input pressure of the actuators to be the target value based on the data read from the sensors. The Bluetooth module transmits signals from a mobile phone to the microcontroller to conduct the corresponding actions, such as hand opening and grasping.

Evaluation of the soft wearable assistive glove

Soft wearable gloves are mainly characterized by their assistive forces and range of motions on the fingers.[17] We therefore conduct a detailed evaluation of our designed glove.

The experimental results in Figure 6c have shown that the thumb-abduction SFPA can abduct the thumb to the functional

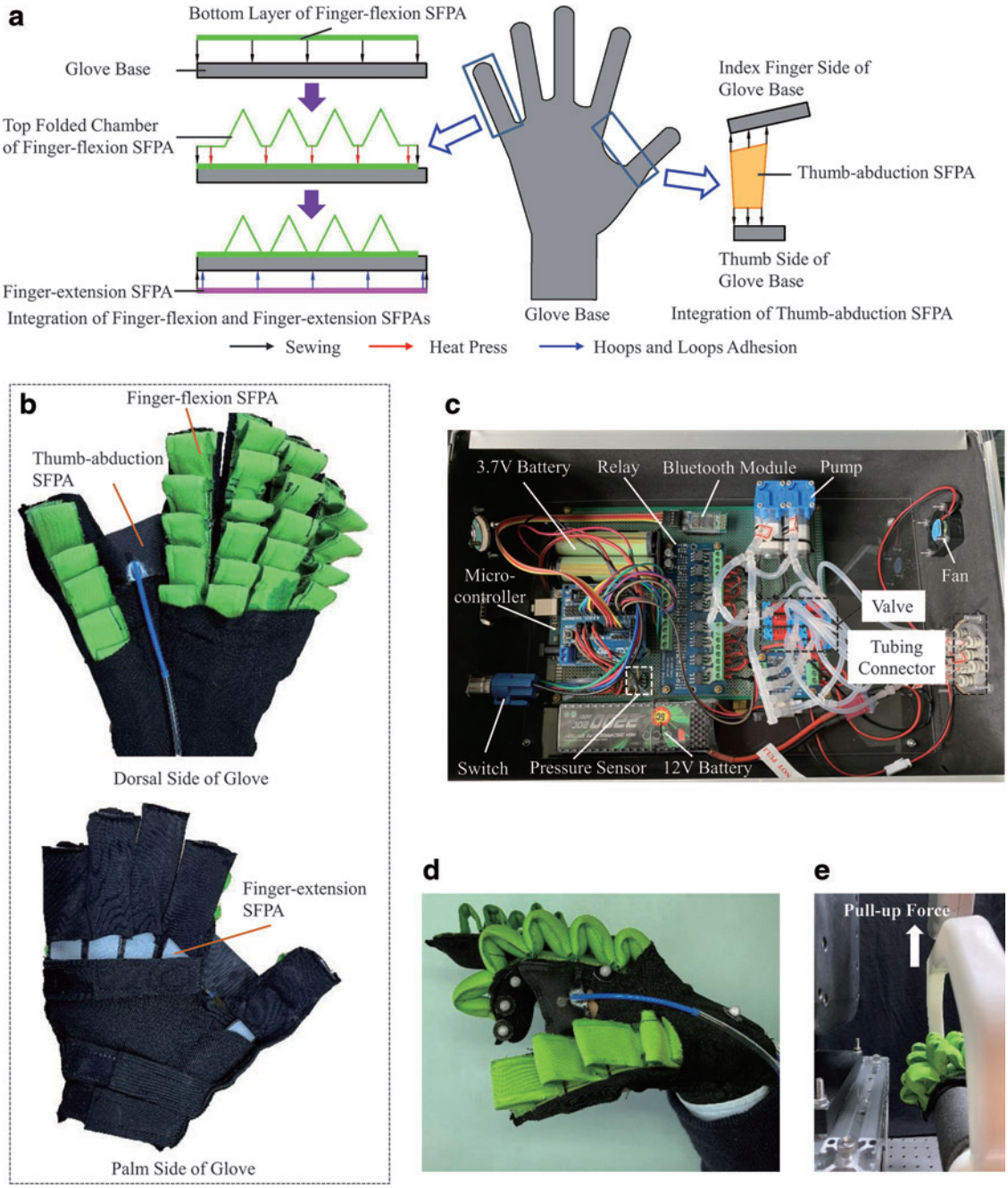

FIG. 10. Integration and characterization of the soft wearable assistive glove. **(a)** The integration process of the thumb-abduction SFPA, and finger-flexion and finger-extension SFPAs into the glove. **(b)** The glove with the integrated SFPAs. **(c)** Control system for the glove. **(d)** Glove assistive index finger flexion evaluation. **(e)** Measurement setup for the normal grasping force for the glove. Color images are available online.

position. The torque required to move a patient's thumb for abduction motion is 0.3 N · m at the carpometacarpal (CMC) joint.[37] The mean lengths of the thumb metacarpal and the thumb proximal phalange are 46.22 and 31.57 mm, respectively.[38] Assuming the assistive abduction force provided by the thumb-abduction SFPA works at the center of the thumb proximal phalange, the force arm is 62 mm. Since the assistive abduction force that the thumb-abduction SFPA can provide is 17.21 N under 140 kPa input pressure (Fig. 6b), the assistive abduction torque at the CMC joint that the thumb-abduction SFPA can generate is $\sim$1.07 N · m, which is sufficient for assisting the thumb abduction motion.

We further measure the flexion angle of the index finger on a healthy volunteer (subject gives written informed consent forms in accordance with the Declaration of Helsinki, and testing is approved by the Ethics Committee of Huashan Hospital, Fudan University) with the assistance of the glove, using the software ImageJ. The input pressure for the finger-flexion SFPA of the index finger is set to be 140 kPa. The test is conducted three times.

It is shown in Figure 10d that the glove can assist the index finger to achieve a 92.3° flexion angle. Since the flexion angles of the PIP joints and the distal IP joints are from 60° to 80° and from 10° to 15°, respectively, in the hand functional position (Fig. 4a), the glove can provide sufficient flexion range of motion in most ADLs. While testing, the thumb-abduction SFPA is simultaneously inflated with 140 kPa pressure. Therefore, the inflated thumb-abduction SFPA causes little interference to the flexion motion of the fingers.

We subsequently measure the assistive grasping force of the glove. As shown in Figure 10e, the finger-flexion SFPAs of the four fingers are pressurized to 140 kPa to grasp a cylinder (of diameter 50 mm). The cylinder is pulled upward by a linear stage (HST-200Z; SIGMAKOKI) at a constant velocity (4 mm/s) until the cylinder is released from the grasp of the glove. The pull-up force, which is the normal grasping force of the glove, is tested and recorded using a dynamometer (ZP-200N; AIGU). The results show that the glove can generate a normal grasping force of 47.9 N. The weights of objects in ADLs are usually less than 1.5 kg.[17] Assuming that the average coefficient of friction between the glove and target objects is 0.5,[22] our glove can provide a large enough grasping force in ADLs.

It is also noted, in a real grasping task, the interaction forces generated by different actuators are distributed and coordinated. An efficient grasp may require force feedbacks via distributed sensing and appropriate control algorithms, which is beyond the scope of this article and will be included in our future work.

The extension motion of the fingers can be impaired by different diseases, such as stroke, spinal cord injury, and brachial plexus injury. The required assistive extension torque at the MCP joints of the four fingers for the stroke patients ranges from 0.5 to 4 N · m.[39] Based on the experimental results in Figure 9d, the finger-extension SFPA on our glove can provide an extension torque of 0.67 N · m with the initial flexion angle being 75° and the input pressure being 140 kPa. With four identical finger-extension SFPAs on the four fingers, the total extension torque reaches 2.68 N · m, which can serve a certain number of patients. Furthermore, the extension torque of the finger-extension SFPA can be scaled by increasing the chamber width and the input pressure.

Preliminary clinical evaluation

Finally, we conduct experiments to verify the feasibility of using our developed glove to assist the patients with hand impairment in accomplishing grasping tasks. We first verify the function of the glove on a healthy volunteer (subject gives written informed consent forms in accordance with the Declaration of Helsinki, and testing is approved by the Ethics Committee of Huashan Hospital, Fudan University).

During the experiment, the volunteer keeps his hand relaxed. As shown in Figure 11a, initially the fingers of the volunteer are naturally flexed, and the thumb is naturally adducted. To assist the volunteer in opening his hand, the finger-extension SFPAs and the thumb-abduction SFPA of the glove are inflated to extend the fingers and abduct the thumb (Fig. 11b). Then the finger-extension SFPAs are deflated, and the finger-flexion SFPAs are inflated to assist the volunteer to grasp the object (Fig. 11c). The working pressure of all the actuators of the glove

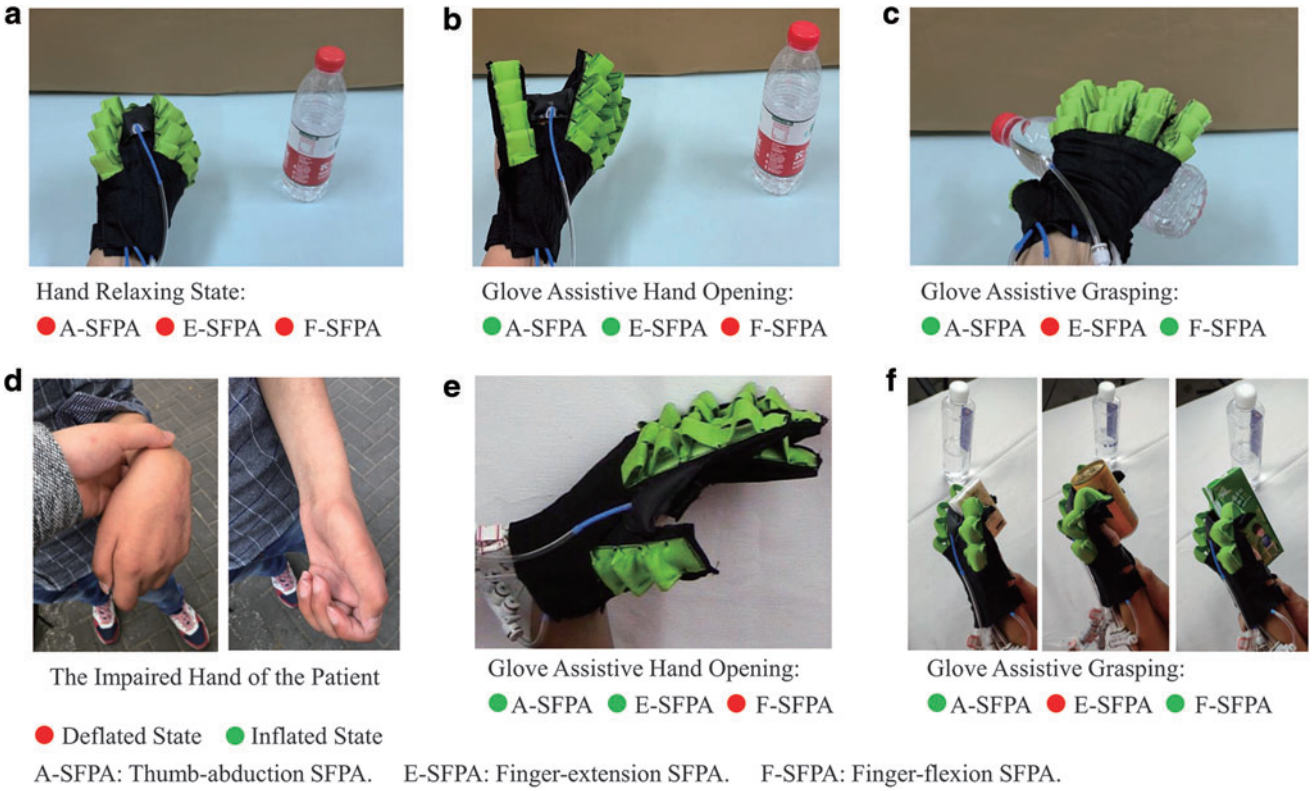

FIG. 11. Grasping assistance evaluation of the soft wearable assistive glove. **(a–c)** Demonstration on a healthy volunteer of the working state of the actuators on the glove in the grasping experiments. **(d–f)** Grasping assistance evaluation of the glove on a brachial plexus injury patient. Color images are available online.

is 140 kPa. We can see that the glove can successfully assist the volunteer to accomplish the grasping task.

We further conduct the grasping experiment on a brachial plexus injury patient (subject gives written informed consent forms in accordance with the Declaration of Helsinki, and testing is approved by the Ethics Committee of Huashan Hospital, Fudan University). The impaired fingers of the patient are clenched and cannot be extended voluntarily (Fig. 11d). The impaired thumb is with adducted distortion and loses abduction motion capability (Fig. 11d). The flexion motion capabilities of the impaired fingers are also severely weakened.

Considering all his fingers are disabled, all the actuators of the soft wearable assistive glove are used to assist the patient in the grasping tests. We fabricate a customized soft wearable assistive glove based on the impaired hand profile of the patient to ensure fitness. The results in Figure 11e and f show that, with an input pressure of 140 kPa, our soft wearable assistive glove can assist the patient to successfully open his hand and grasp several daily objects of different shapes.

Conclusion

In this work, we present the design, modeling, and evaluation of a class of SFPAs for soft wearable assistive gloves. We first systematically study the mechanical properties of various fabrics that provide a novel palette of materials for the SFPAs. By proper material selection and geometric structuring, we design finger-flexion and finger-extension SFPAs, and particularly a thumb-abduction SFPA. A mathematical model is then developed to investigate their mechanical behaviors upon pressurization and parametric studies are conducted to improve their actuation performance in terms of the output motions and forces.

We finally design and fabricate a soft wearable glove that can successfully assist a brachial plexus injury patient in opening his hand and accomplishing several grasping tasks in ADLs. Our work paves the way for future applications of soft wearable devices in hand assistance and rehabilitation.

This work mainly focuses on the mechanical design and performance of the SFPAs and their integration into a soft wearable assistive glove, providing a versatile platform for further research on hand rehabilitation training and assistance. In future work, we will exploit electroencephalogram and electromyographic signals to enable the patients to voluntarily control the glove in hand rehabilitation training and ADL tasks. Flexible force sensors and strain sensors will be integrated into the glove to monitor the assistive force and range of motion, so as to provide proper grasping force and posture feedback.

Acknowledgments

The authors thank the brachial plexus injury patient and the healthy volunteer for their participation in the study.

Author Disclosure Statement

No competing financial interests exist.

Funding Information

This work was supported by the National Natural Science Foundation of China (Grant Nos. 91948302 and 91848204), Innovative research team of high-level local universities in Shanghai, and Shanghai Jiao Tong University Scientific and Technological Innovation Funds.

References

1. Gu G, Zou J, Zhao R, *et al.* Soft wall-climbing robots. Sci Robot 2018;3:2874.
2. Gu GY, Zhu J, Zhu LM, *et al.* A survey on dielectric elastomer actuators for soft robots. Bioinspir Biomim 2017; 12:011003.
3. Zhang YF, Zhang N, Hingorani H, *et al.* Fast-response, stiffness-tunable soft actuator by hybrid multimaterial 3D printing. Adv Funct Mater 2019;29:1806698.
4. Gassert R, Dietz V. Rehabilitation robots for the treatment of sensorimotor deficits: a neurophysiological perspective. J Neuroeng Rehabil 2018;15:46.
5. Mosadegh B, Polygerinos P, Keplinger C, *et al.* Pneumatic networks for soft robotics that actuate rapidly. Adv Funct Mater. 2014;24:2163–2170.
6. Hassan T, Cianchetti M, Moatamedi M, *et al.* Finite-element modeling and design of a pneumatic braided muscle actuator with multifunctional capabilities. IEEE ASME Trans Mechatron 2018;24:109–119.
7. Wang T, Ge L, Gu G. Programmable design of soft pneu-net actuators with oblique chambers can generate coupled bending and twisting motions. Sens Actuators A Phys 2018; 271:131–138.
8. Ge L, Dong L, Wang D, *et al.* A digital light processing 3D printer for fast and high-precision fabrication of soft pneumatic actuators. Sens Actuators A Phys 2018;273:285–292.
9. Ge L, Wang T, Zhang N, *et al.* Fabrication of soft pneumatic network actuators with oblique chambers. J Vis Exp 2018:e58277.
10. Connolly F, Polygerinos P, Walsh CJ, *et al.* Mechanical programming of soft actuators by varying fiber angle. Soft Robot 2015;2:26–32.
11. Connolly F, Walsh CJ, Bertoldi K. Automatic design of fiber-reinforced soft actuators for trajectory matching. Proc Natl Acad Sci U S A 2017;114:51–56.
12. Drotman D, Ishida M, Jadhav S, *et al.* Application-driven design of soft, 3-D printed, pneumatic actuators with bellows. IEEE ASME Trans Mechatron 2018;24:78–87.
13. Zhang H, Kumar AS, Chen F, *et al.* Topology optimized multimaterial soft fingers for applications on grippers, rehabilitation, and artificial hands. IEEE ASME Trans Mechatron 2018;24:120–131.
14. Deimel R, Brock O. A novel type of compliant and underactuated robotic hand for dexterous grasping. Int J Rob Res 2016;35:161–185.
15. Chu CY, Patterson RM. Soft robotic devices for hand rehabilitation and assistance: a narrative review. J Neuroeng Rehabil 2018;15:9.
16. Connelly L, Jia Y, Toro ML, *et al.* A pneumatic glove and immersive virtual reality environment for hand rehabilitative training after stroke. IEEE Trans Neural Syst Rehabil Eng 2010;18:551–559.
17. Polygerinos P, Wang Z, Galloway KC, *et al.* Soft robotic glove for combined assistance and at-home rehabilitation. Rob Auton Syst 2015;73:135–143.
18. Yap HK, Ang BW, Lim JH, *et al.* A fabric-regulated soft robotic glove with user intent detection using EMG and RFID for hand assistive application. In: 2016 IEEE International Conference on Robotics and Automation, Stockholm, Sweden, 2016, pp. 3537–3542.

19. Yap HK, Lim JH, Nasrallah F, *et al.* Design and preliminary feasibility study of a soft robotic glove for hand function assistance in stroke survivors. Front Neurosci 2017;11:547.
20. Heung KH, Tong RK, Lau AT, *et al.* Robotic glove with soft-elastic composite actuators for assisting activities of daily living. Soft Robot 2019;6:289–304.
21. Yap HK, Khin PM, Koh TH, *et al.* A fully fabric-based bidirectional soft robotic glove for assistance and rehabilitation of hand impaired patients. IEEE Robot Autom Lett 2017;2:1383–1390.
22. Cappello L, Galloway KC, Sanan S, *et al.* Exploiting textile mechanical anisotropy for fabric-based pneumatic actuators. Soft Robot 2018;5:662–674.
23. Cappello L, Meyer JT, Galloway KC, *et al.* Assisting hand function after spinal cord injury with a fabric-based soft robotic glove. J Neuroeng Rehabil 2018;15:59.
24. Connolly F, Wagner DA, Walsh CJ, *et al.* Sew-free anisotropic textile composites for rapid design and manufacturing of soft wearable robots. Extreme Mech Lett 2019;27:52–58.
25. Feix T, Pawlik R, Schmiedmayer H-B, *et al.* A comprehensive grasp taxonomy. In: Robotics, science and systems: workshop on understanding the human hand for advancing robotic manipulation, Washington, USA, 2009, pp. 2–3.
26. de Kraker M, Selles RW, Schreuders TA, *et al.* The Pollexograph: a new device for palmar abduction measurements of the thumb. J Hand Ther 2009;22:271–276.
27. Sondhelm WS. 4—Technical fabric structures—1. Woven fabrics. In: Horrocks AR, Anand SC, eds. Handbook of Technical Textiles. Cambridge: Woodhead Publishing, 2000, pp. 62–94.
28. Anand SC. 5—Technical fabric structures—2. Knitted fabrics. In: Horrocks AR, Anand SC, eds. Handbook of Technical Textiles. Cambridge: Woodhead Publishing, 2000, pp. 95–129.
29. Duhovic M, Bhattacharyya D. Simulating the deformation mechanisms of knitted fabric composites. Compos Part A Appl Sci Manuf 2006;37:1897–1915.
30. Tascan M, Vaughn EA. Effects of fiber denier, fiber cross-sectional shape and fabric density on acoustical behavior of vertically lapped nonwoven fabrics. J Eng Fiber Fabr 2008; 3:155892500800300206.
31. Suarez-Escobar M, Rendon-Velez E. An overview of robotic/mechanical devices for post-stroke thumb rehabilitation. Disabil Rehabil Assist Technol 2018;13:683–703.
32. Kapandji AI. Clinical evaluation of the thumb's opposition. J Hand Ther 1992;5:102–106.
33. Xu D. Shougongneng xiufu chongjian waike jiepouxue [surgical anatomy for reconstruction of the hand]. Beijing, China: Renmin weisheng chubanshe, 1996.
34. Lin J, Zheng H-P, Xu Y-Q, *et al*. Special Type of Finger Replantation: Techniques and Cases. Singapore: Springer, 2018.
35. Glaser R, Caccese V. Experimental methods to determine in-plane material properties of polyurethane-coated nylon fabric. J Text I 2013;104:682–698.
36. Bauchau O, Craig J. Structural Analysis. Dordrecht, the Netherlands: Springer, 2009.
37. Lambercy O, Schröder D, Zwicker S, *et al.* Design of a thumb exoskeleton for hand rehabilitation. In: Proceedings of the 7th International Convention on Rehabilitation Engineering and Assistive Technology, Singapore, Singapore, 2013, p. 41.
38. Buryanov A, Kotiuk V. Proportions of hand segments. Int J Morphol 2010;28:755–758.
39. Kamper DG, Rymer WZ. Quantitative features of the stretch response of extrinsic finger muscles in hemiparetic stroke. Muscle Nerve 2000;23:954–961.

Address correspondence to:
Guoying Gu
Robotics Institute
School of Mechanical Engineering
Shanghai Jiao Tong University
Shanghai 200240
China

E-mail: guguoying@sjtu.edu.cn